# Nano-analytical electron microscopy reveals fundamental insights into human cardiovascular tissue calcification

Supplementary table 1: Aortic valve donor information (n=32).

Patient age (yr)	57±11 (range: 38 to 81)
Patient sex	65% male, 35% female
Patient cause of death	21% Sub-arachnoid, 36% Intracranial haemorrhage, 7% Myocardial infarction, 4% Cardiac arrest, 32% Other
Cause of rejection for valve transplant	83% Excess of atheroma, 7% Damage to aorta wall, 10% Unknown

Supplementary table 2: Donor information for mitral valve, aorta and coronary artery tissue (n = 17 mitral valves, n = 14 coronary arteries and n = 22 aortas).

|	Mitral	Arteries (Coronary + aorta)
Patient age (yr)	Adults 56±8 (range: 38 to 73) plus 5 children	55±11 (range: 31 to 73)
Cause of death or cause of valve removal	39% Rheumatic fever, 22% Intracranial haemorrhage,11% Sub-arachnoid, 6% Cardiac arrest, 6% Myocardial infarction, 16% Other	35% Intracranial haemorrhage, 15% Sub-arachnoid, 10% Myocardial infarction, 10% Cardiac arrest, 5% Rheumatic fever, 25% Other
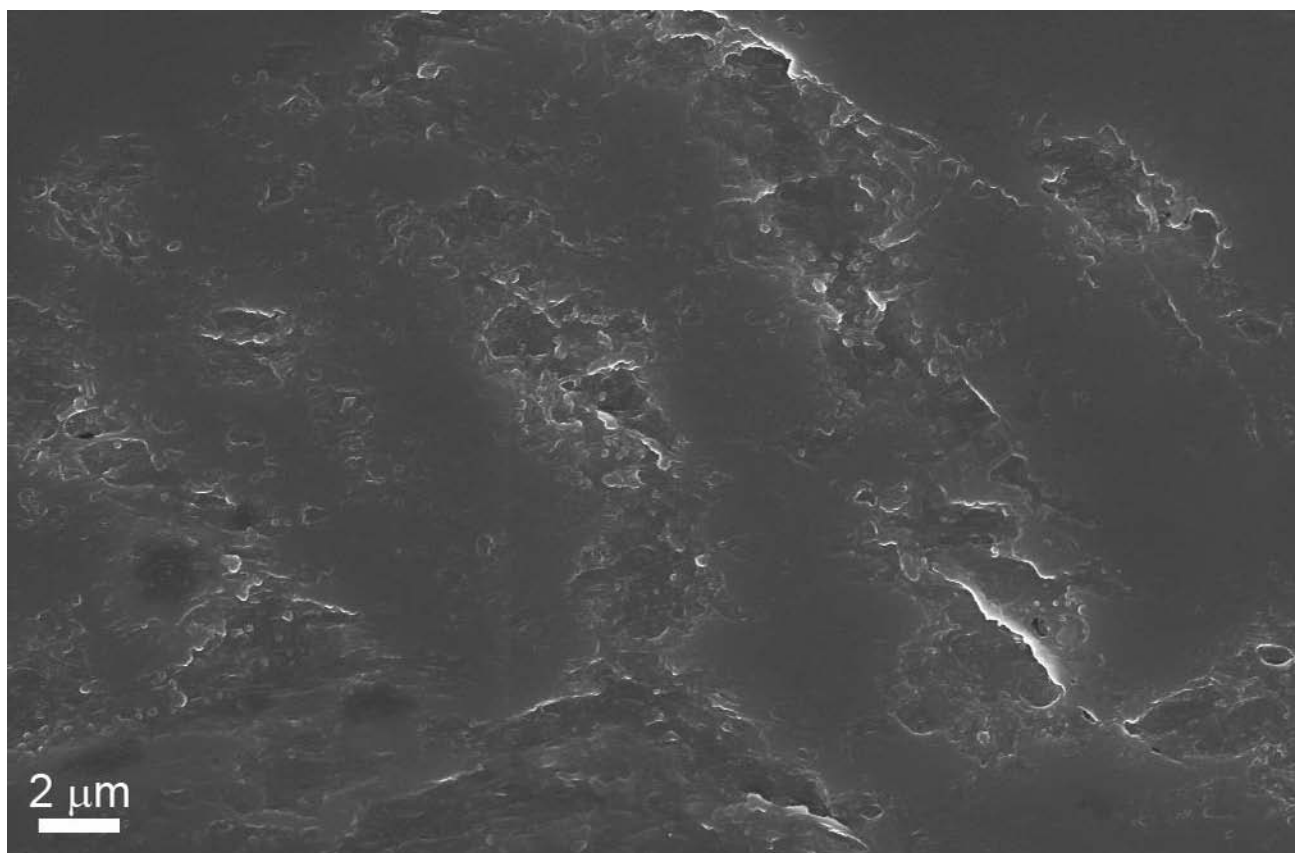
Supplementary Figure 1: Representative scanning electron micrograph of the surface of an aortic valve that was free from macroscopic calcific lesions on either the valve or surrounding tissue. The valve was rejected for transplant as a homograft because of physical damage.
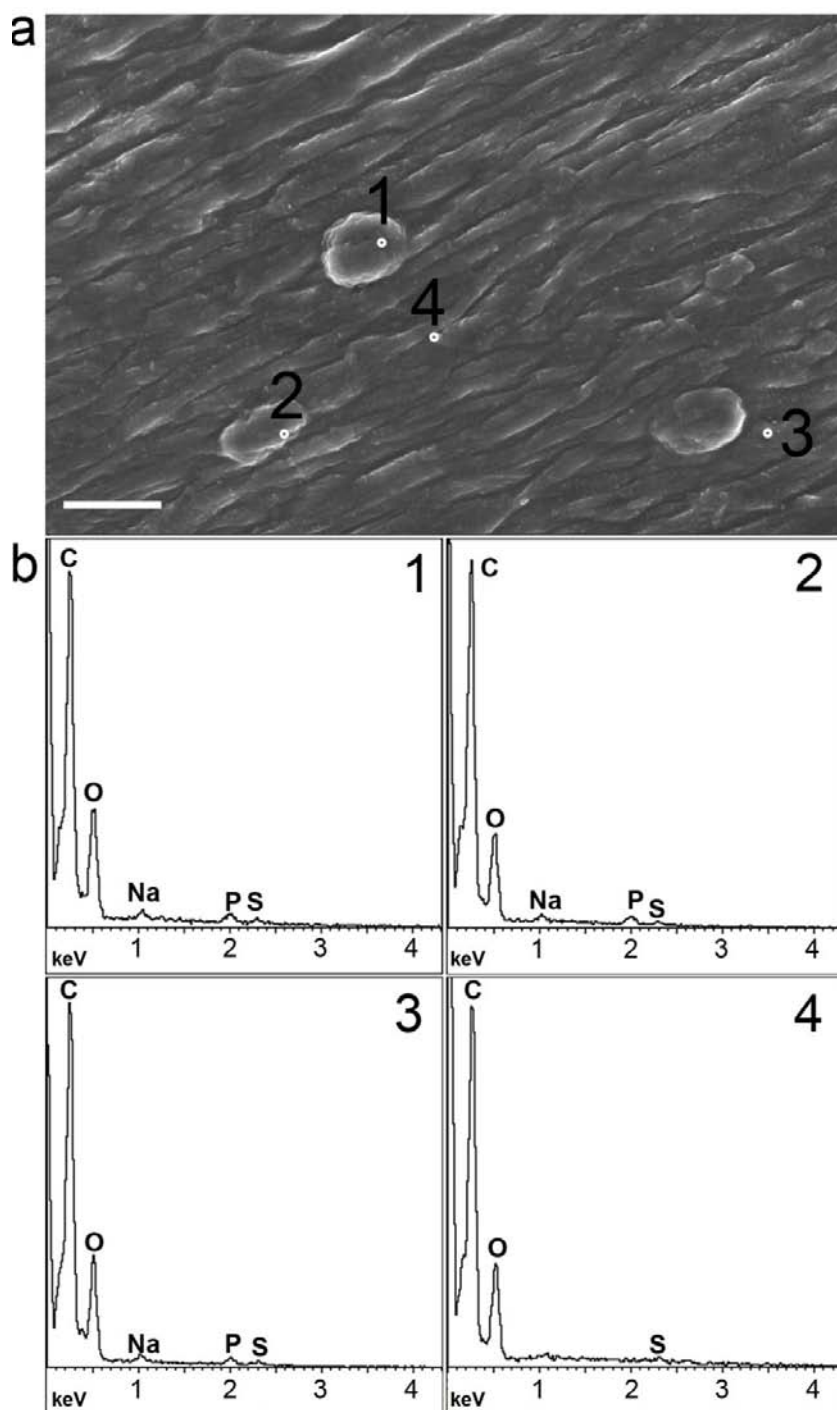
Supplementary Figure 2: Elemental analysis of an aortic valve surface that was free from macroscopic calcific lesions on either the valve or surrounding tissue. Valve was rejected for transplant because of physical damage. **a** Scanning electron microscopy image of aortic valve tissue surface. Numbered circles indicate the regions subsampled by energy-dispersive X-ray spectroscopy (EDS). **b** EDS spectra of the regions indicated in **a**. Note that all areas sampled lacked calcium and phosphorous and were organic in composition. Scale bar = 10 μm.
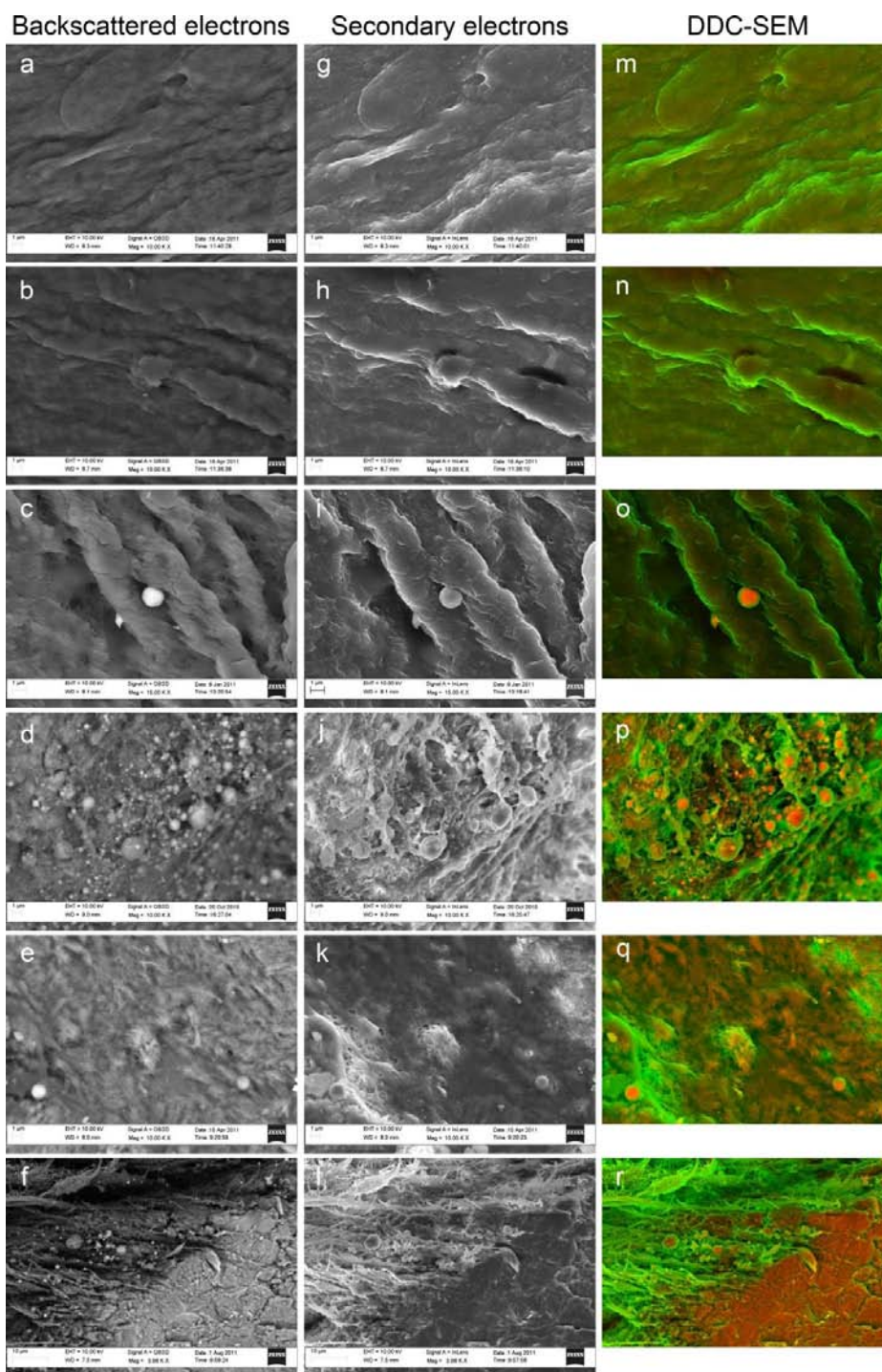
Supplementary Figure 3: Image processing steps utilized to create the density-dependent colour scanning electron micrographs (DDC-SEM) presented in Figures 1 and 5, which differ from standard "false color" SEM images. Using the "stack" command in ImageJ software, SEM micrographs acquired in backscatter mode (**a**, **b**, **c**, **d**, **e** and **f**) were merged with SEM micrographs obtained from the identical region, but acquired in secondary electron mode (**g**, **h**, **i**, **j** and **l**). The combined images were then converted into a single RGB image using ImageJ command "stack to RGD" with the backscatter image assigned to the red channel and the secondary electron mode image stacked on the green channel. This technique allowed for simultaneous visualization of both topography and density in a single image. The final output, images **m**, **n**, **o**, **p**, **q** and **r,** show denser material in orange/red and the less dense material in green.
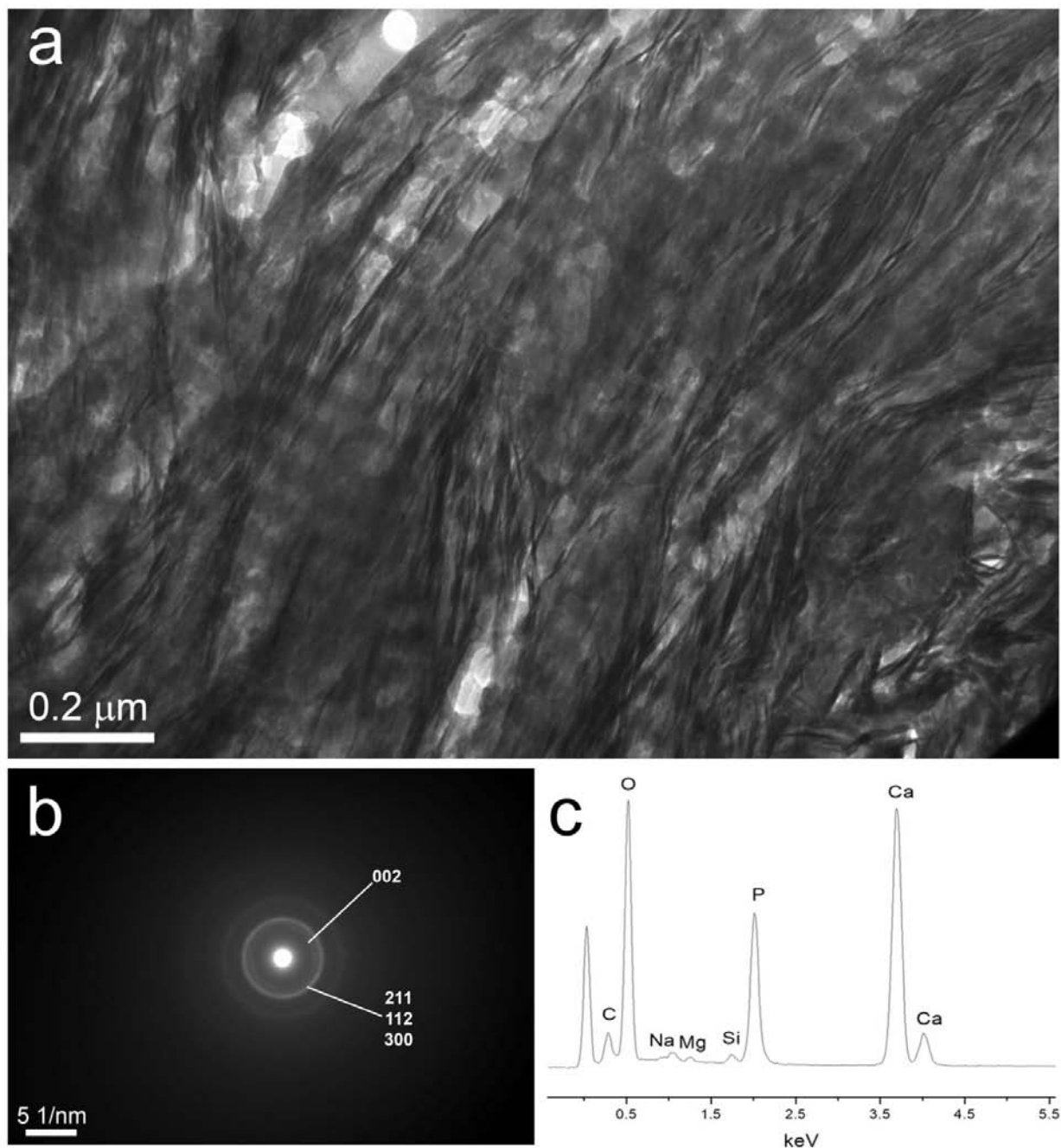
Supplementary Figure 4: Analyses of human bone samples obtained from patients undergoing total hip arthroplasty procedures. **a** Transmission electron microscopy image of bone sectioned with a focussed ion beam showing typical banded collagen and apatite crystals which comprise the bone matrix. **b** Selected area electron diffraction from region imaged in **a**, which reveals a poorly crystalline apatite pattern typical of native bone. The 211, 112 and 300 planes are indicated. Scale bar = 0.05 nm^{-1}. **c** Energy-dispersive X-ray spectroscopy spectrum from the region imaged in **a**, which highlights bone's elemental composition.
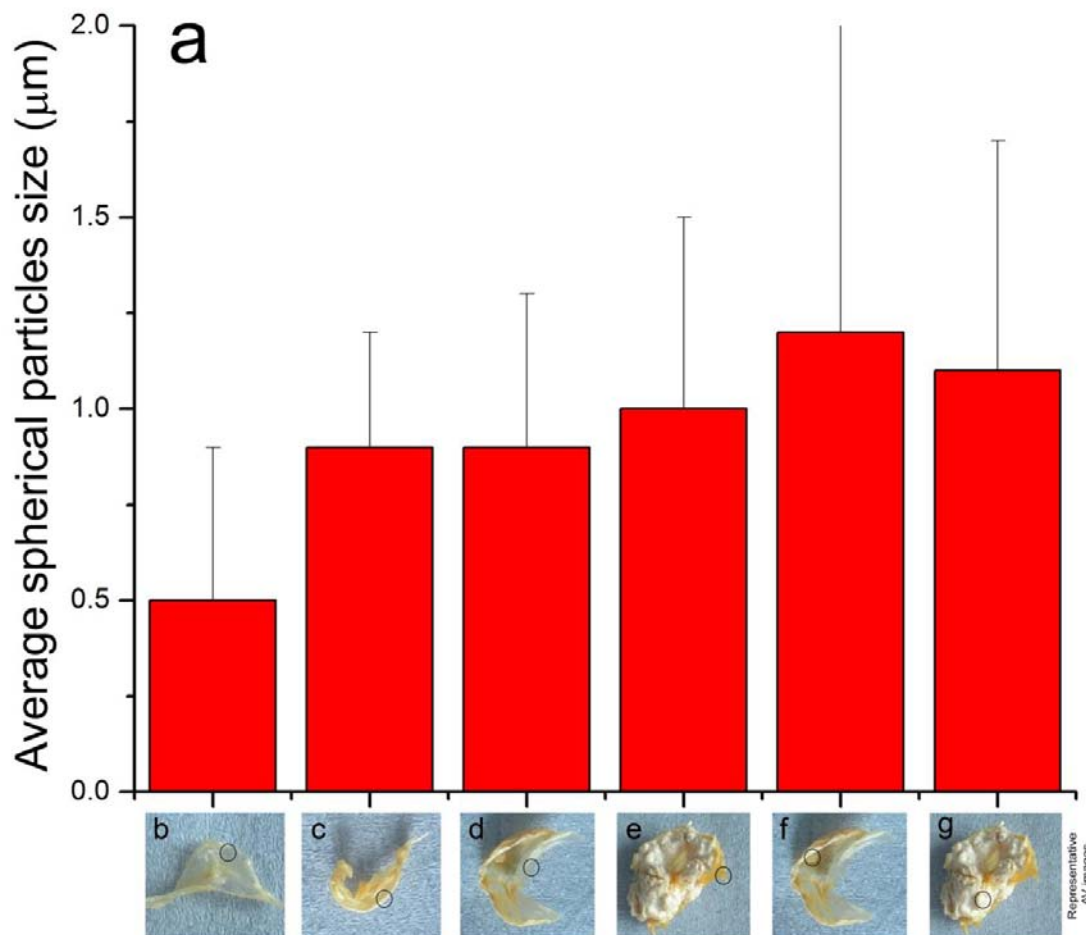
Supplementary Figure 5: Histogram of the average size of spherical particles. Representative images of AV are categorized by presence and extensiveness of calcific lesions. Sub-sampled regions indicated in circles. Category b is comprised of AV that did not present any macroscopically observable calcific lesions on AV or in surrounding tissue (aorta and coronary arteries). c represents AV without macroscopically observable calcification on AV, but with macroscopically observable calcific lesions on surrounding tissues. d includes analyses carried out on non-calcified areas of AV which presented calcific lesions in other areas of the AV. e includes analyses carried out on non-calcified areas of AV which were heavily calcified in other areas. f identifies structures on macroscopically observable AV calcific lesions. g includes analyses carried out on calcific lesions from heavily calcified AV. Approximately 350 images were obtained from each of the 55 regions examined in AV from 32 patients.
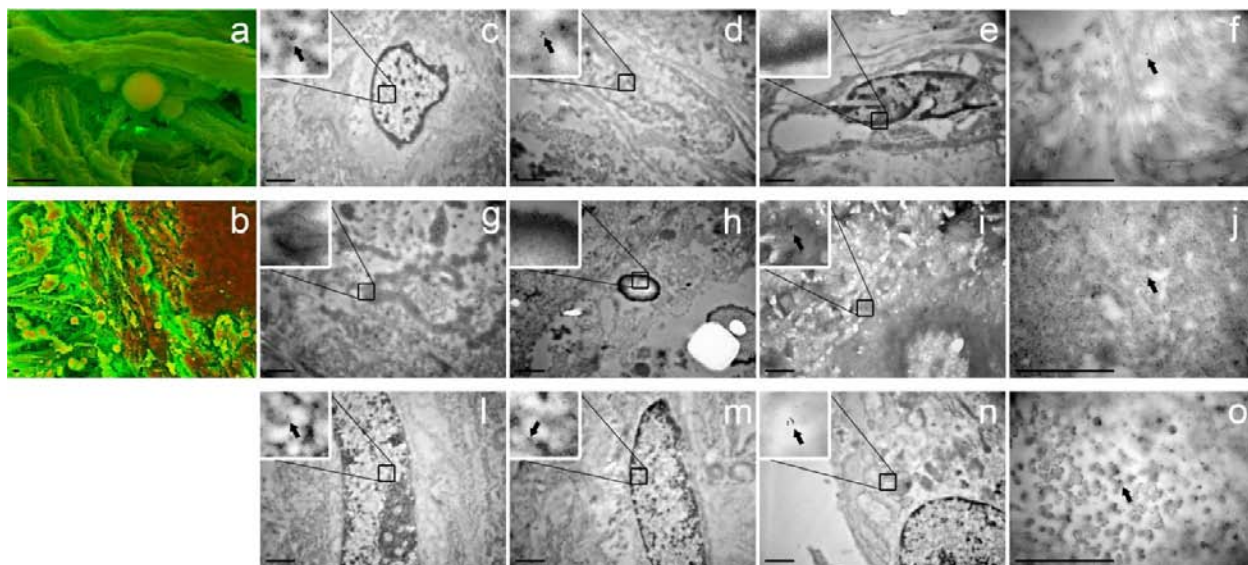
Supplementary Figure 6: Immunogold labelling in aorta and aortic valve tissue and the murine osteoblast cells line MC3T3-E1. **a/b** Representative density-dependent colour scanning electron micrographs of aortic valve tissue presenting either spherical particles alone **a**, or compact calcification and spherical particles associated with calcific lesions **b**. **c-f** Transmission electron microscopy (TEM) images of tissue presenting only dense spherical particles immunogold labelled for Runx2 (**c**), SP7 (**d**), osteocalcin (**e**) and type I collagen (**f**). Note that tissues show positive labelling for the early osteoblast transcription factors Runx2 and Sp7; labelling was localized to cell nuclei. **g-j** TEM images of tissue presenting compact calcification and spherical particles immunogold labelled for Runx2 (**g**), SP7 (**h**), osteocalcin (**i**) and type I collagen (**j**). Tissues labelled positively for the bone-specific protein osteocalcin. It was difficult to identify cell nuclei in the dense, less cellular material associated with calcific lesions. **l-o** TEM images of MC3T3-E1 mouse osteoblast cultures, immunogold labelled for Runx2 (**l**), SP7 (**m**), osteocalcin (**n**) and type I collagen (**o**). MC3T3-E1 cultures label positively for Runx2, SP7, and osteocalcin. All tissues and cell cultures labelled positively for type I collagen; gold labelling was clearly associated with fibrous protein that had banding patterns typical of mammalian collagen. Gold nanoparticles are evident in the insets and highligted by arrows. Scale bar = 1 μm.
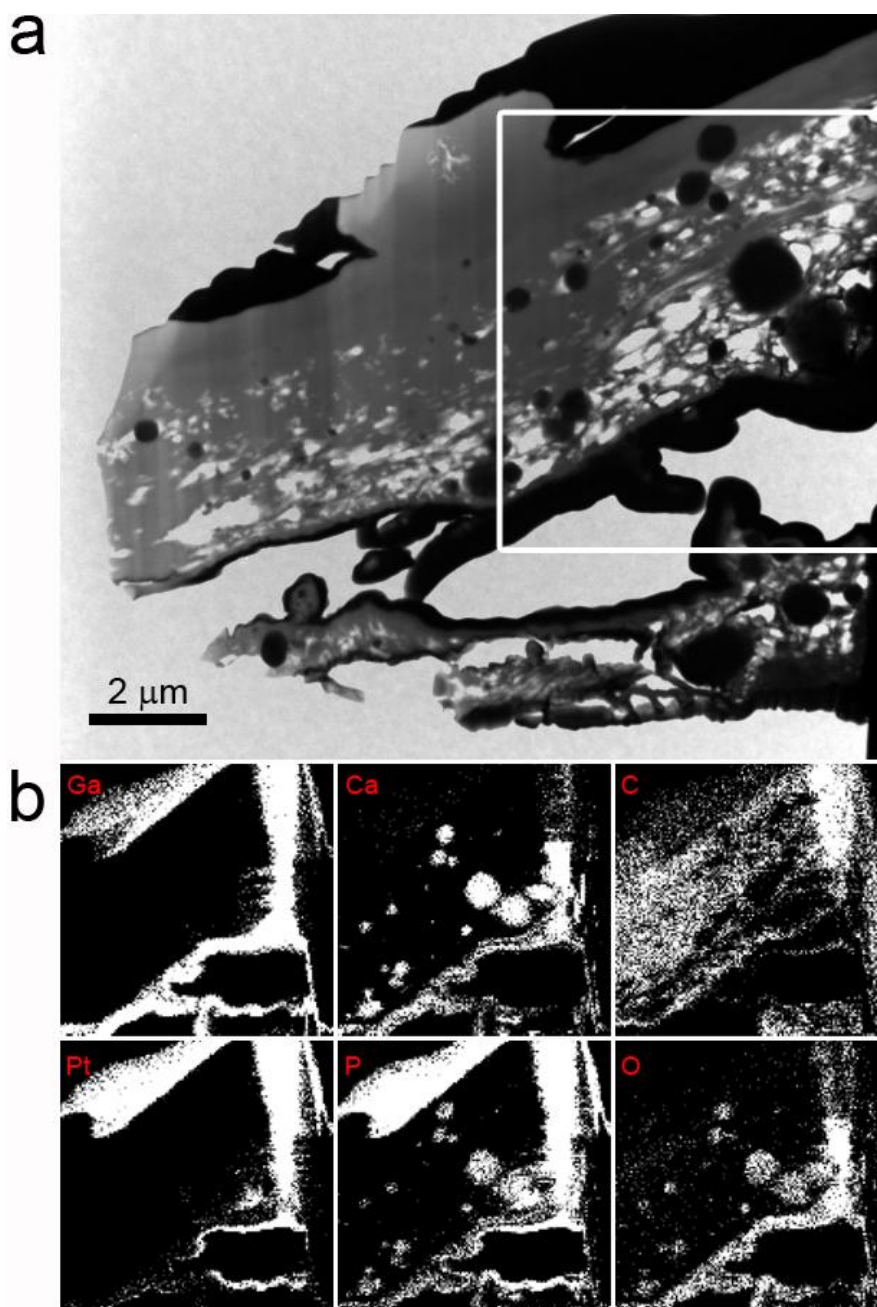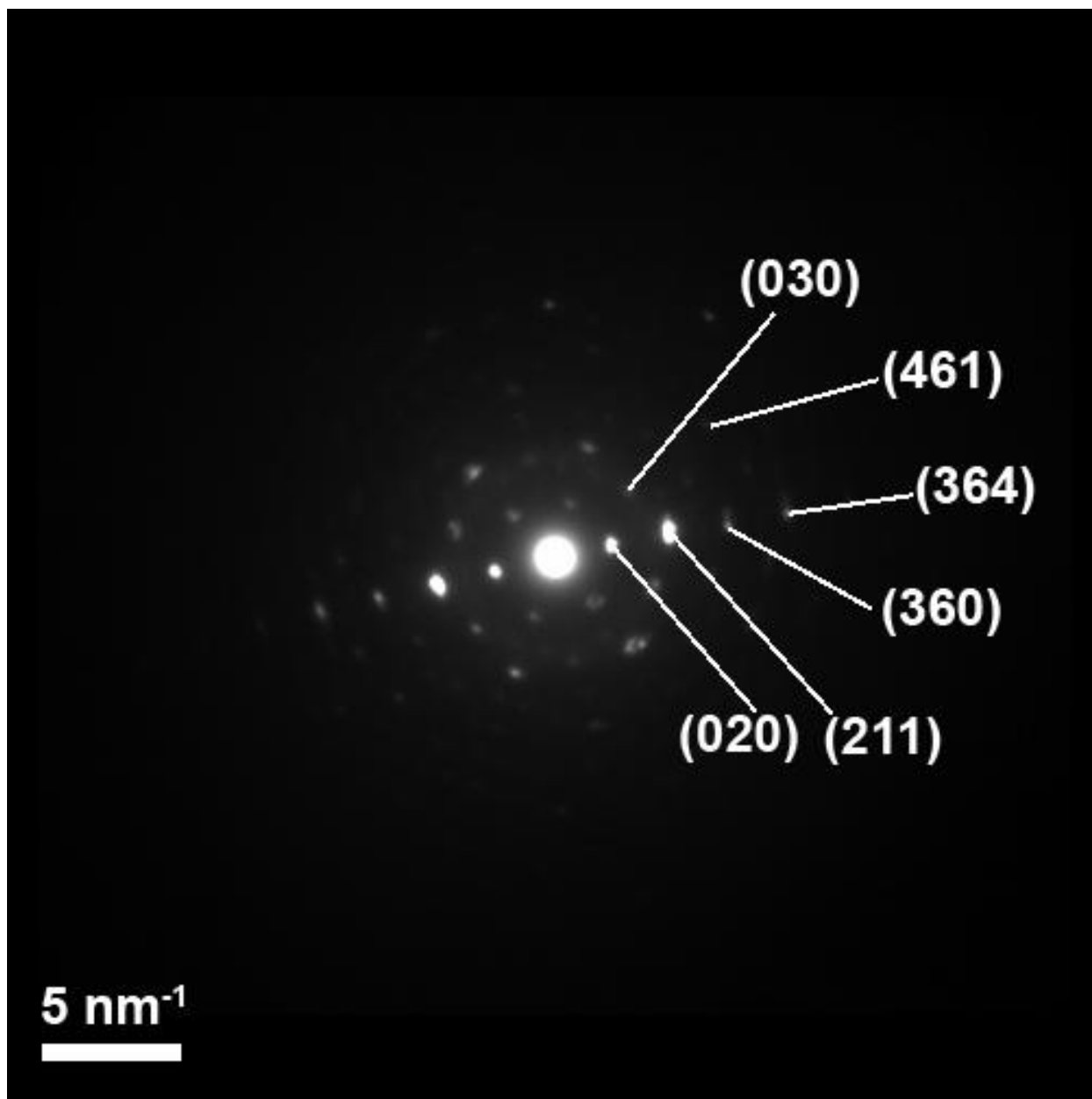
Supplementary Figure 7: a Transmission electron micrograph of a calcific lesion extracted from an aortic valve with a focussed ion beam. **b** Energy-dispersive X-ray spectroscopy elemental maps obtained from the region within the square shown in **a**. Maps show the distribution of gallium (Ga), calcium (Ca), carbon (C), platinum (Pt), phosphorus (P) and oxygen (O) in the sample. Spheres are rich in calcium and phosphorus but lack detectable levels of carbon. Gallium was used as the source for the ion beam. Platinum was used to attach the sample to the sample holder (as can be seen in the right-hand region of **a**, and to protect the surface during milling.
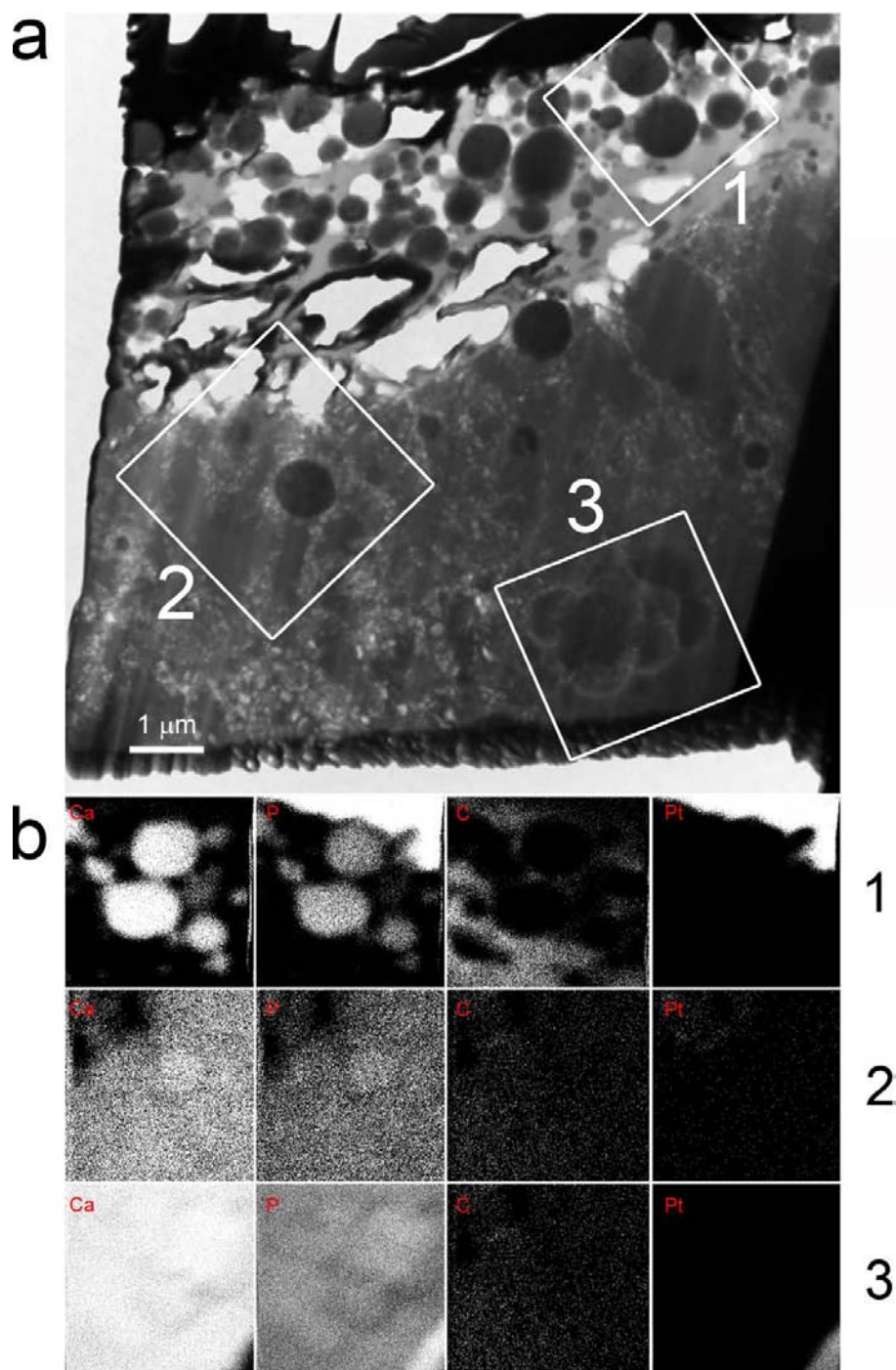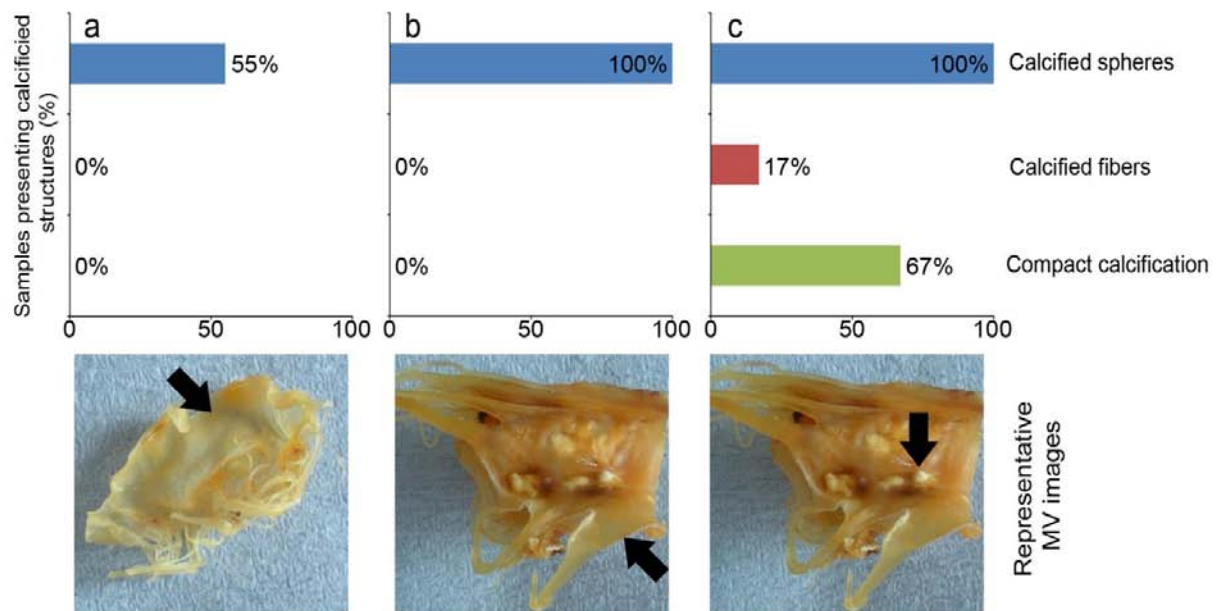
Supplementary Figure 8: a Transmission electron micrograph of the surface of a calcific lesion extracted from an aortic valve with a focussed ion beam. **b** Energy-dispersive X-ray spectroscopy elemental maps obtained from the regions within squares 1, 2 and 3, shown in **a**. Maps show the distribution of calcium (Ca), phosphorus (P), carbon (C), and platinum (Pt) in the sample. Calcium- and phosphorus-rich spherical particles are evident when embedded within an organic matrix (1), but are more difficult to discern by elemental mapping when surrounded by the dense calcium- and phosphorus-containing compact material that comprised much of calcific lesions (2 and 3). Platinum was used to attach the sample to the sample holder and to protect the surface during milling (as seen in the top portion of **a**).
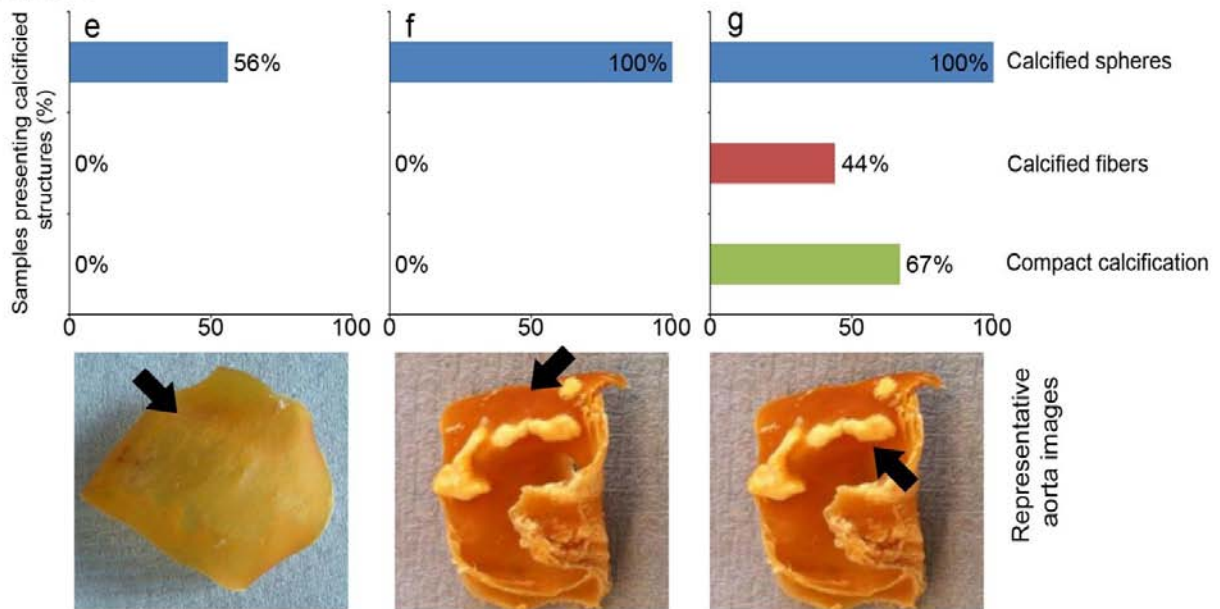
Supplementary Figure 9: Electron diffraction pattern recorded by transmission electron microscopy of a dense spherical particle extracted from a calcific lesion on an aortic valve using a focused ion beam. The Miller indices corresponding to hydroxyapatite are indicated.

Supplementary Figure 10: Histogram denoting the prevalence of dense calcium- and phosphorus-containing structures on the surface of mitral valve and artery tissue samples. Representative images of tissue are categorized by presence or lack of calcific lesions. Sub-sampled regions indicated by arrows. Categories **a** and **e** comprise tissue that did not present any macroscopically observable calcific lesions. **b** and **f** includes analyses carried out on non-calcified areas from samples which had macroscopically detectable calcific lesions in other areas of the tissue. **c** and **g** includes analyses carried out on calcific lesions. *Analysis carried out in 22 aortas and 14 coronary arteries.
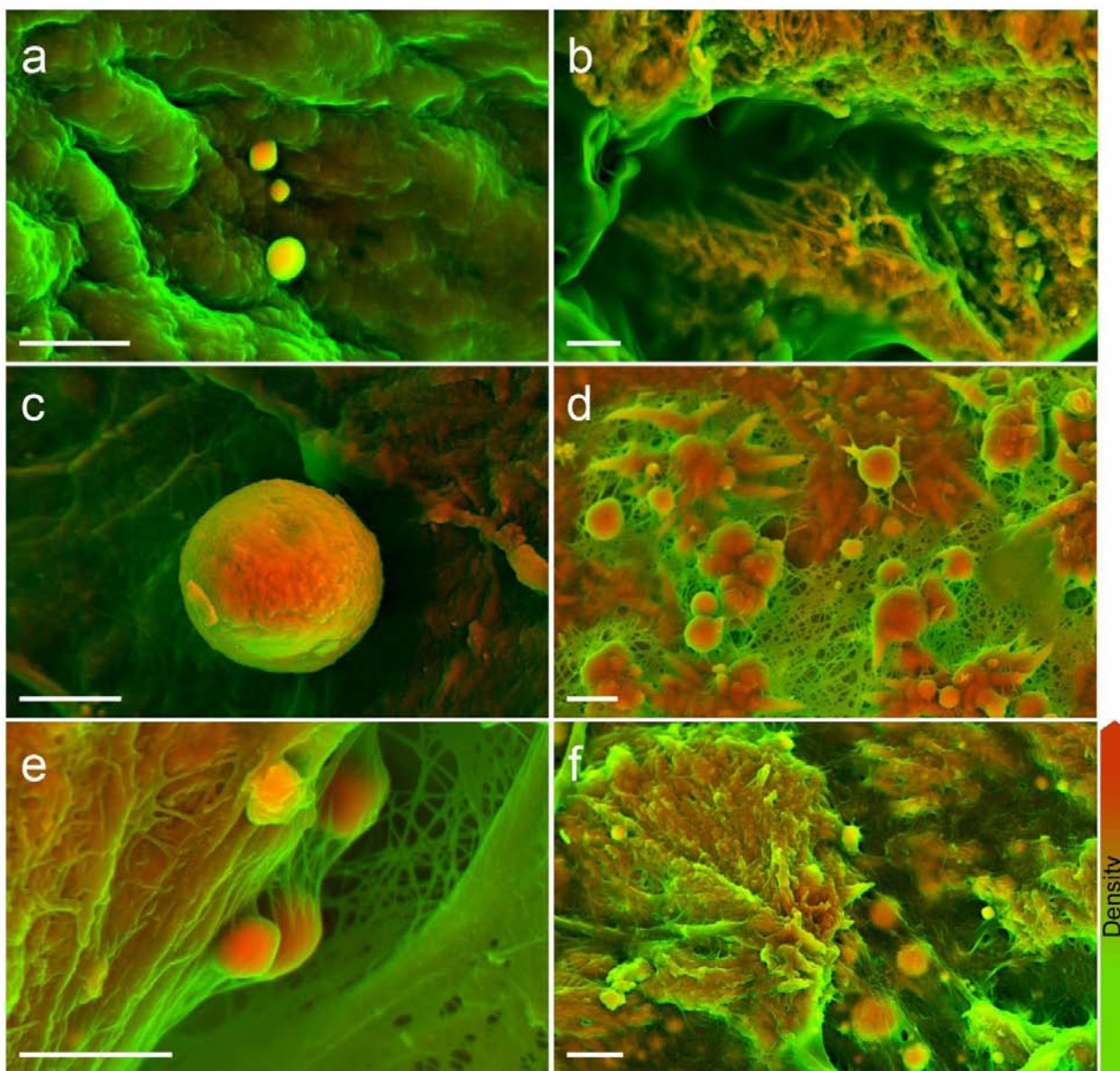
Supplementary Figure 11: Density-dependent colour scanning electron micrographs of mitral valve, aorta and coronary artery tissues. **a** Mitral valve with notable dense spherical particles. **b** Mitral valve presenting dense spherical particles and fibers. **c** Aorta with notable dense spherical particles. **d** Aorta presenting dense spherical particles and fibers. **e** Coronary artery presenting dense spherical particles. **f** Coronary artery presenting dense spherical particles and fibers. Scale bar = 3 μm.
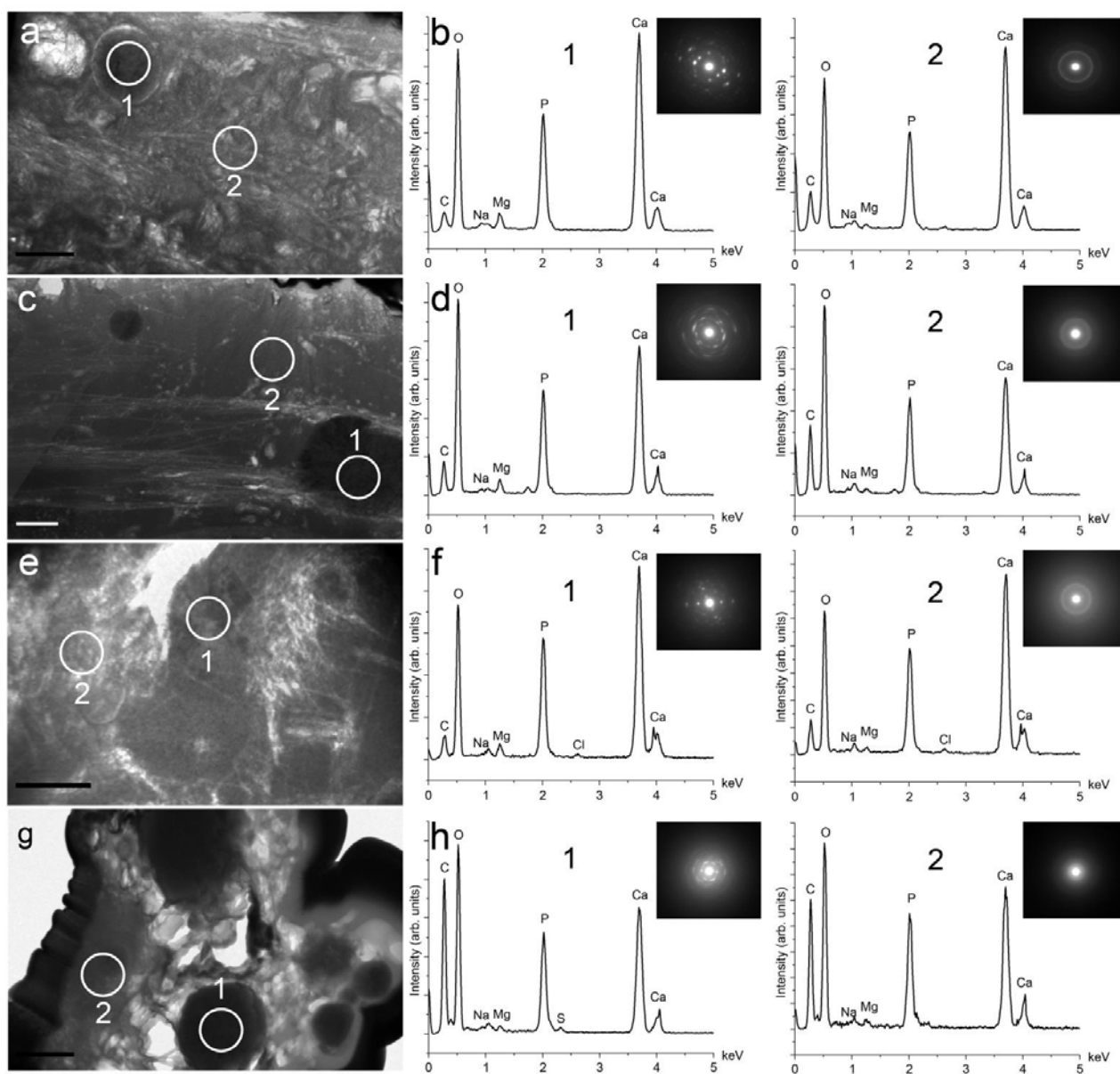
Supplementary Figure 12: Transmission electron microscopy (TEM), energy-dispersive X-ray spectroscopy (EDS) and selected area electron diffraction (SAED) of aorta, coronary artery, mitral and aortic valve calcific lesions sectioned by a focussed ion beam (FIB). **a, c, e** and **g** TEM of calcific lesions sectioned by FIB in **a** aorta, **c** coronary artery, **e** mitral valve and **g** aortic valve tissue. Scale bar = 2 μm. Spherical particles are evident embedded within the matrix. **b**, **d**, **f** and **h** show EDS spectra and SAED patterns of the regions numbered in **a, c, e** and **g,** respectively. EDS spectra demonstrate that all of the sampled regions were rich in calcium and phosphorus. Spectra numbered 1 were obtained from dense spherical particles; SAED demonstrates their highly crystalline nature. Spectra numbered 2 are regions that contained a poorly crystalline calcium phosphate. Note that the peak for magnesium is consistently stronger on the spherical particles when compared to that obtained from regions containing poorly crystalline calcium phosphate.